Design and Development of a Solar-Powered IoT-Based Energy Consumption Monitoring System

Anuar Jaafar[1*], Aiman Haqeem Ahmad Tarmizi[1], Haziezol Helmi Mohd Yusof[1], Kamaliah Hanim Samhudi Kamil[2], Siti Aisyah Anas[1], Noor Shahida Mohd Kasim[1], Abd Majid Darsono[1]

[1]Centre for Telecommunication Research and Innovation (CeTRI), Fakulti Teknologi dan Kejuruteraan Elektronik dan Komputer, Universiti Teknikal Malaysia Melaka

[2]Jabatan Kejuruteraan Elektrik, Politeknik Port Dickson, KM 14, Jalan Pantai, 71050 Si Rusa, Negeri Sembilan, Malaysia.

DOI: https://doi.org/10.47772/IJRISS.2026.100700366

Received: 20 July 2026; Accepted: 25 July 2026; Published: 01 August 2026

ABSTRACT

Residential energy conservation is frequently hindered by a lack of real-time visibility into usage, widening the "behavior-action gap" between daily electricity utilization and delayed monthly utility statements. This paper presents the development of a low-cost, open-source, residential solar-powered Internet of Things (IoT) monitoring system. The proposed architecture segments data collection tasks into a Direct Current (DC) renewable generation node and an Alternating Current (AC) appliance-level consumption interface using dual ESP32 microcontrollers. The system collects data from precision inline INA226 shunt sensors on the solar and battery storage paths, alongside a ZMPT101B transformer and an SCT-013 current transformer wrapped in a physical 5-turn wire loop to lift low-power current boundaries above standard resolution floors. Telemetry is streamed asynchronously via Message Queuing Telemetry Transport (MQTT) over a cloud HiveMQ broker. To optimize edge node efficiency, chronological timestamping is completely decoupled from the hardware layer and managed server-side upon database ingestion into InfluxDB. Real-time and historical analytics are visualised using a centralized Grafana web dashboard interface. Experimental results show that the hardware sensing layer maintained high measurement precision, yielding low absolute errors ($V_{error} \leq 0.38\%$ and $I_{error} \leq 32\%$) and successfully resolving low-power household standby states down to single-digit wattages (e.g., 9W). The event-driven alert system achieved zero-latency multi-tier warnings, verifying that the proposed framework delivers an accessible, high-fidelity sub-metering platform for urban electrification programs.

Keywords: Solar Energy, Internet of Things (IoT), Energy Consumption Monitoring.

INTRODUCTION

As domestic electricity costs rise and climate targets tighten, optimization of household consumption has become an international priority. Occupant energy habits represent a highly variable and significant determinant of net grid strain. However, a persistent "behavior-action gap" exists where residential consumers acknowledge environmental pressures but fail to adopt conservation practices. This disconnect stems directly from the invisible nature of electricity and the significant delay between daily consumption actions and historical monthly utility billing.

To overcome this lack of visibility, modern Home Energy Management Systems (HEMS) attempt to capture electrical data. Nevertheless, contemporary residential options suffer from a split landscape. Whole-house utility monitors only trace total aggregate electricity footmarks, placing an immense analytical burden on the user to identify specific high-consumption appliances. Conversely, standalone consumer smart plugs focus narrowly on accessible plug loads, excluding fixed high-consumption infrastructure like lighting and HVAC.

A critical integration gap exists because standard hardware systems treat solar photovoltaic (PV) generation tracking and household sub-metering as isolated, separate domains. This prevents residents from practicing efficient "load shifting"—the process of moving high-power household tasks to peak solar availability periods to increase direct self-consumption and maximize energy independence.

To bridge this divide, this research designs and implements an integrated, open-source, dual-node residential solar monitoring prototype. The system splits tracking constraints across low-voltage Direct Current (DC) renewable paths and isolated single-phase Alternating Current (AC) residential terminal configurations using dual ESP32 processing edge nodes. High-frequency telemetry updates stream over standard Message Queuing Telemetry Transport (MQTT) pipelines, bypassing edge-level time synchronization routines by enforcing a high-precision server-side time ingestion model within an index-optimized InfluxDB time-series database management system (TSDBMS).

Related Work

Non-Invasive Sensing and Fundamentals of Electrical Quantification

The foundational layer of any intelligent Home Energy Management System (HEMS) relies on the precise and safe acquisition of raw electrical parameters across alternating current (AC) and direct current (DC) domains [1]. In single-phase AC residential circuits, electrical utilization is defined by three interrelated properties: Root-Mean-Square voltage (Vrms), Root-Mean-Square current (Irms), and real active power (P) [3]. Real power represents the actual work performed by an active domestic load to convert energy into heat, mechanical rotation, or light, calculated as the product of the voltage, current, and the cosine of the phase angle ($\cos \varphi$) separating their waveforms—conceptually defined as the power factor (PF) [5].

To capture these volatile waveforms safely without creating destructive electrical arcs or requiring invasive physical splicing of live grid conductors, modern IoT nodes rely predominantly on galvanic isolation sensing methods [4]. Alternating current is tracked non-invasively using split-core current transformers (CTs), such as the SCT-013 module, which clamp externally around a single current-carrying conductor to measure its shifting magnetic fields [5]. These transformers step down primary current flows into a lower, safe secondary current path, which is subsequently converted into an analog voltage wave using an integrated burden resistor before processing by a microcontroller's Analog-to-Digital Converter (ADC) [4]. Concurrently, isolated potential step-down transformers, such as the ZMPT101B module, condition the high-voltage AC grid supply into lower signal voltages safely [5].

For renewable direct current paths, including solar photovoltaic (PV) arrays and battery storage banks, precision measurements are executed using inline shunt-based sensor integrated circuits like the INA226 [1]. These devices sense micro-voltage drops across a low-resistance precision resistor placed directly in the power path, outputting high-accuracy digital data to a microcontroller via an I2C serial communication interface [1].

Classification and Structural Limitations of Contemporary HEMS

The current structural landscape of residential energy management is heavily divided into specific categories based on deployment scope, functionality, and data access, each exhibiting critical limitations:

- Utility Smart Meters: Acting as the primary commercial gate between the consumer and national power grids, smart meters log billing data and enable time-of-use pricing adjustments [5]. However, utility portals present data at low temporal resolutions—frequently restricted to hourly or daily blocks—and prioritize provider billing requirements over localized consumer insight [6]. This structural limitation makes smart meters unsuitable for granular appliance habit tracking or real-time diagnostic awareness [3].
- Whole-House Monitors: Installed at the main breaker panel using aggregate non-invasive sensors, these systems map the collective electricity consumption of an entire residence [6]. While they provide a clear overall view of a household's energy footprint, they generally lack the granularity to break down individual device usage, leaving users to guess the specific source of unexplained energy spikes [3].
- Plug-Load Monitors: Comprising localized smart plugs or hardware terminal interfaces, these modules focus on tracking individual appliances [6]. While they are highly accurate at measuring specific standalone

ISSN No. 2454-6186 | DOI: 10.47772/IJRISS | Volume X Issue VII July 2026

devices like entertainment systems or water heaters, their narrow scope excludes major integrated household loads, such as centralized lighting branches or fixed HVAC units, failing to provide a holistic house-wide view [4].

- Solar PV Monitoring Systems: Dedicated commercial platforms track solar photovoltaic output properties, including irradiance profiles and panel temperatures, to observe long-term system health [2]. However, these portals operate in complete isolation from household consumption data [2][7].

This systematic isolation between generation tracking and consumption sub-metering forms a major operational gap in residential energy management [1]. Without an affordable, unified interface that maps both electrical paths simultaneously, homeowners cannot practice active "load shifting"—the process of moving high-energy tasks to peak solar generation hours to increase direct self-consumption, minimize expensive evening grid draws, and maximize true energy independence [1].

Resource Optimization and Edge-to-Gateway Middleware Processing

To bridge these separate monitoring fields within an affordable framework, the implementation of Internet of Things (IoT) network structures relies on distinct functional layers: sensing, connectivity, data processing, and visualization [4]. Selecting the appropriate microcontroller and network protocol forms the critical bridge between physical edge sensing and centralized cloud storage [5]. The ESP32 microcontroller serves as a premier engine for home tracking nodes due to its dual-core processing architecture, high clock frequencies up to 240 MHz, and native Wi-Fi peripherals [2]. This dual-core topology allows the edge node to delegate high-frequency analog sampling routines to one processing core while concurrently maintaining network sockets and data transmission threads on the secondary core without creating processing bottlenecks [2].

Furthermore, continuous high-frequency sampling creates a major data logging strain if microcontrollers are forced to manage heavy internal clock-tracking tasks or execute manual synchronization routines with external Network Time Protocol (NTP) servers via UDP [3]. Recent advancements in IoT middleware prove that decoupling temporal tracking from resource-constrained edge hardware significantly optimizes runtime stability [3]. By deploying edge nodes as stateless telemetry engines that serialize filtered parameters into lightweight JSON strings, data can be broadcasted instantly using the Message Queuing Telemetry Transport (MQTT) transport protocol over a broker channel [4].

Responsibility for chronological indexing shifts entirely onto the ingestion tier of a server-side Time-Series Database Management System (TSDBMS) like InfluxDB [3]. The database automatically appends a high-precision timestamp using the host server's master clock the exact millisecond a payload hits the write endpoint [3]. This design architecture minimizes edge firmware weight, protects local memory stacks, and creates a reliable, synchronized index for downstream dashboard rendering via Grafana [3].

Table 1: Summary of Sensors, Features and System Functions

Study Type	Strength	Limitation	Relation to Proposed Work
Traditional HEMS	Real-time appliance sub-metering	Isolated tracking; lacks information	Integrates AC appliance loads with DC solar/battery tracking on a single interface
Cloud Tracking	Remote visualization and logging over Wi-Fi	Heavy network dependency and cloud API reliance	Employs open-source, self-hosted Node-RED middleware for resilient data processing.

ISSN No. 2454-6186 | DOI: 10.47772/IJRISS | Volume X Issue VII July 2026

Edge Nodes	Low-latency local script execution	Computational strain and complex edge clock-sync loops	Uses stateless edge transmitters with server-side time ingestion into InfluxDB

METHODOLOGY

System Architecture

To circumvent the high deployment costs and complex software overhead typical of industrial-grade tracking equipment, the proposed architecture maps residential power dynamics across two separate hardware domains managed under a centralized, open-source server pipeline. The structural design splits telemetry collection into a low-voltage Direct Current (DC) renewable pathway (Node 1) and an independent, high-voltage single-phase Alternating Current (AC) load monitoring interface (Node 2). This structural decoupling establishes clean operational processing boundaries and isolates volatile AC inverter switching noise from precision DC shunt lines.

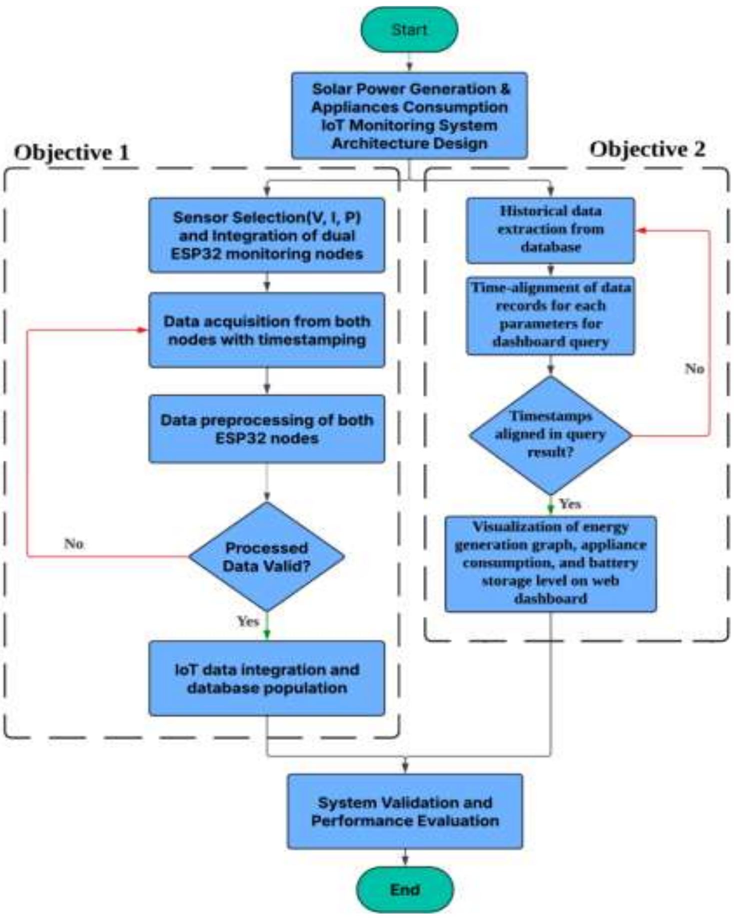

Figure 1. Proposed Solar-Powered IoT Monitoring System architecture

Segmented Edge Node Configurations

- Node 1 (Generation & Storage Domain): Driven by an independent ESP32 microcontroller, Node 1 acquires data from two inline 16-bit INA226 current/power monitors to track the solar photovoltaic array and the LiFePO4 battery storage reservoir concurrently. To completely eliminate communication bus collisions and delays induced by sensor clock-stretching, the monitors are separated into separate native hardware I2C registries using the microcontroller's wire routing matrix:

ISSN No. 2454-6186 | DOI: 10.47772/IJRISS | Volume X Issue VII July 2026

- Solar PV Track (Wire Bus): Configured on default pins GPIO 21 (SDA) and GPIO 22 (SCL), polling across a precision shunt resistor (RShunt_Solar = 0.1Ω) to map voltage variations and generated current.

- Battery Bank Track (Wire1 Bus): Mapped to alternate pins GPIO 16 (SDA) and GPIO 17 (SCL), sensing drops across a low-resistance shunt (RShunt_Battery = 0.01Ω) to minimize active power dissipation losses (I2R) along the core discharge path.

- Node 2 (AC Load Consumption Domain): Isolated down-line from a pure sine wave power inverter stage, Node 2 captures electrical properties from a single localized plug outlet utilizing a ZMPT101B potential transformer paired with a non-invasive split-core SCT-013 current transformer. The internal 12-bit SAR ADC on the ESP32 samples incoming waves at high frequency. To safely process negative voltage waves without damaging chip architecture, the incoming signals pass through external divider networks injecting a +1.65V DC mid-bias shift to capture full waves within the positive 0V to 3.3V logic envelope. The summary of the proposed system was tabulated in Table 2.

Table 2. Summarizes the sensors used in the proposed system.

Parameter	Sensor / Circuit	Interface	Function
Solar Voltage (DC)	INA226 #1	I2C (Wire1)	Monitors the DC voltage output from the solar PV
Solar Current (DC)	INA226 #1	I2C (Wire1)	Measures the current from the solar PV
Battery Voltage (DC)	INA226 #2	I2C (Wire0)	Tracks the battery voltage level
Battery Discharge Current(DC)	INA226 #2	I2C (Wire0)	Tracks discharge current of the battery.
Load Voltage (AC)	ZMPT101B	ADC	Measures the AC mains voltage flowing through the load
Appliance Current (AC)	SCT-013	ADC	Track current drawn by household loads.

Firmware Preprocessing and Mathematical Filtering

Root-Mean-Square (RMS) metrics are calculated directly on the edge by sweeping analog parameters through 400 sequential samples separated by a tight 250 microseconds delay register:

$$Vrms = \frac{\sqrt{\frac{1}{400}\sum_{n=1}^{400} \quad (Vanalog_n - offsetV)^2}}{vCal}$$

$$Irms = \frac{\sqrt{\frac{1}{400}\sum_{n=1}^{400} \quad (Ianalog_n - offsetVI}}{iCal}$$

where offsetV and offsetI define dynamic mathematical zero-baselines compiled during an initialization loop at boot to negate drifting hardware offset shifts.

To overcome physical resolution floor bottlenecks when clamping inductive sensors onto low-power standby hardware, a physical 5-turn wire loop wraps around the SCT-013 clamp core, multiplying the field density by 5 to lift the parameter clear of native hardware noise floors. The edge firmware divides incoming metrics by 5 to downscale properties back to single-wire values before serialization. Additionally, a strict software gate limits data pollution: if line potential falls below 10.0V or current falls below a 15.0mA floor, the parameters force automatically to a clean 0.0, cutting off background phantom loads. Active power calculations are completed by multiplying the calibrated parameters ($P_{real} = V_{rms} * I_{rms}$) assuming a stable resistive baseline (PF = 1.00) when load presence is captured.

Ingestion Pipeline and Database Alignment Middleware

Edge parameters are packed into stateless JSON string structures and published asynchronously over secured Wi-Fi client links via Message Queuing Telemetry Transport (MQTT) over a cloud HiveMQ broker using Quality of Service Level 1 (QoS 1) handshake rules. This configuration keeps edge nodes highly efficient by completely removing Network Time Protocol (NTP) server clock loops from the microcontroller firmware.

A server-side Node-RED middleware engine maintains a wildcard subscription to decode incoming payloads into clean metrics using Line Protocol formatting strings within low millisecond execution windows. Payload points are written straight to InfluxDB, which automatically indexes rows down to the millisecond using the master clock of the host server upon write ingestion.

For historical analytics rendered on the Grafana frontend interface, data records pass through a secondary database alignment validation loop. Because nodes publish asynchronously, the historical pipeline applies an aggregateWindow() script to downsample dense parameter points into unified timeline tracking buckets using mean data filters. Any prolonged transmission drop voids or router retransmission delays are smoothly bridged via query-tier linear interpolation filling parameters (fill(linear)), preventing the multi-axis dashboard panels from fracturing or dropping unexpectedly to zero.

Automated Event-Driven Protective Alert Logic

Proactive resource protection is integrated directly into the Node-RED middleware broker engine. Under active discharge testing conditions, the engine continuously checks incoming battery metrics against conditional threshold boundaries. To shield the battery bank from harmful deep discharge states, a throttled state-machine code block monitors capacity triggers. Once capacity transits below the initial 20% boundary, the engine pushes a low-latency push notification string through the Telegram Bot API stating "Capacity has dropped below 20%!". The state machine automatically locks subsequent alert retransmissions to prevent redundant notification flooding until capacity breaches the next consecutive 5% marker.

RESULTS AND DISCUSSION

Sensor Validation

Steady-state testing evaluated the accuracy of both sensing nodes against reference bench instruments. The low-voltage direct current monitoring section controlled by Node 1 used two independent INA226 sensor modules to track the 12W solar panel and the 12V LiFePO4 battery storage. To verify accuracy, a handheld digital multimeter was used to take live parallel benchmark readings of the bus voltages during the active testing session. The maximum voltage tracking error remained extremely low, proving the solar node is properly calibrated.

During data collection, the measured operating voltage of the solar panel stayed consistently around 13V instead of matching the panel's nominal open-circuit rating of 18V. This behavior is due to the operation of the system's 20A PWM charge controller. A PWM controller regulates battery charging by acting as a direct switch that links the solar array directly to the battery storage medium. Because it lacks voltage-bucking conversion circuits, it clamps the higher potential voltage of the solar panel down to match the active voltage of the 12V LiFePO4 battery. The INA226 sensor successfully captured this loading effect in real time, proving

ISSN No. 2454-6186 | DOI: 10.47772/IJRISS | Volume X Issue VII July 2026

that the direct current data collection layer accurately tracks true physical circuit behaviors rather than theoretical values.

For the battery storage subsystem, the baseline voltage tracking error cross-checked by the multimeter remained well under 1.0 percent across all conditions, validating the storage monitoring calibration. Measured voltage levels for both the solar array and the battery storage subsystem were nearly identical, hovering generally around 13V. This behavior accurately reflects the physical circuit dynamics created by the system's 20A PWM charge controller which continuously pairs the solar array's output terminal to the battery's chemical potential line during active charging phases.

Unlike the low-voltage direct current subsystem, physical verification of the alternating current consumption tracking layer managed by Node 2 introduces distinct operational and safety constraints. For the physical hardware validation, a handheld digital multimeter was used to safely take live parallel benchmark readings of the alternating current mains voltage directly at the plug point interface. The percentage error remained well below 1.0 percent, proving that the alternating current voltage tracking node is highly accurate and properly calibrated.

To calibrate and verify the alternating current measurements safely without inline metering, a known reference load method was implemented using standalone 3W, 9W, and 11W LED bulbs. Because small electronics operate at very low amperages, a physical 5-turn wire loop was wrapped through the sensor clamp core to multiply the physical magnetic field passing through the sensor by 5, converting the primary measurement range to a highly sensitive scale. The resulting percentage error for all calculated parameters remained well below the acceptable threshold for micro-power electronics, confirming the reliability of the non-invasive clamping loop and proving the system's ability to cleanly resolve low-power appliance loads down to single-digit wattages.

Table 3. Solar PV Array Voltage Validation

INA226 Solar Voltage Reading (V)	Multimeter Reading (V)	Absolute Error	Percentage Error (%)
13.18	13.2	0.02	0.15
13.12	13.09	0.03	0.23
13.2	13.22	0.02	0.15
13.04	13.08	0.04	0.3
12.93	12.97	0.04	0.3
13.18	13.2	0.02	0.15

Table 4. Battery Storage Voltage Validation

INA226 Solar Voltage Reading (V)	Multimeter Reading (V)	Absolute Error	Percentage Error (%)
13.12	13.16	0.04	0.3

ISSN No. 2454-6186 | DOI: 10.47772/IJRISS | Volume X Issue VII July 2026

13.07	13.02	0.05	0.38
13.09	13.13	0.04	0.3
13.01	12.99	0.02	0.15
12.96	12.95	0.01	0.08
13.12	13.16	0.04	0.3

Table 5. AC Load Voltage Validation

ZMPT101B Voltage Reading (V)	Multimeter Reading (V)	Absolute Error	Percentage Error (%)
226.83	226.49	0.34	0.15
228.49	229.91	1.42	0.62
231.62	231.48	0.14	0.06
233.91	232.09	1.82	0.78
234.55	235.56	1.01	0.43
226.83	226.49	0.34	0.15

Ingestion Performance and Query-Tier Alignment Analytics

The network layer's performance was audited by tracking the behavior of telemetry packets transmitted by the independent edge microcontrollers. Node 1 and Node 2 successfully functioned as lightweight MQTT clients, packaging their respective processed variables into stateless JSON arrays without attaching edge-generated time metrics. Both nodes communicated successfully over the local network via secured TCP sockets to the cloud-hosted HiveMQ broker on standard port 1883. By enforcing an MQTT Quality of Service Level 1 protocol for all publication payloads, the transport pipeline demonstrated high structural resilience, achieving a 100 percent data delivery rate.

To verify that the database engine successfully coordinates independent, asynchronous data channels onto a unified timeline without relying on edge clock-tracking components, the structural consistency of the ingested logs was reviewed. A review of the raw database records confirmed that the InfluxDB engine successfully intercepted incoming payloads from both nodes, instantly appending a high-precision write-time timestamp under the master time column index using the host server's internal reference clock. Cross-examination of the simultaneous logging sheets showed that the asynchronous metrics from both nodes remained bound cleanly within the maximum network variance boundary of 2000 milliseconds. This server-side synchronization mechanism effectively eliminated edge-level timing drift and transit-induced data skews.

The database layout was evaluated by directly auditing the structural logs populated within the backend measurement buckets. The time-series ledger tables successfully verified that the InfluxDB engine intercepted incoming payloads from both independent edge microcontrollers without data corruption. It appended high-

ISSN No. 2454-6186 | DOI: 10.47772/IJRISS | Volume X Issue VII July 2026

precision write-time timestamps using the host server's reference clock, organizing the direct current and alternating current tracking fields cleanly under a single master time column index.

To prevent these asynchronous entry shifts from causing misalignments on dashboard charts, the query layer's synchronization logic successfully executed temporal grouping rules using specialized time-bucketing functions to force individual data records into matching, sequential time windows. When a temporary data gap occurred due to a brief network retransmission pause, the query pipeline automatically applied linear interpolation rules, cleanly drawing a continuous bridge across the empty indices to maintain structural continuity across the timeline and prevent charts from dropping to zero or breaking unexpectedly.

The operational execution of this automated process was audited under active load testing. The smartphone application interface successfully captured the live message stream generated by the custom alert bot channel. When critical depletion limits were crossed, the execution engine successfully managed alert throttling to shield the user from redundant message flooding while confirming the precise capacity percentage and mapping the next expected safety threshold line to the prosumer terminal.

Figure 2. Node-RED flow showing MQTT data ingestion, JSON string parsing, and parallel database notification branching

The experimental data collected from the dual-node monitoring infrastructure validates the underlying engineering design choices of the system. The narrow voltage tracking errors documented in the direct current sensing subsystem confirm that high-resolution inline shunt monitoring via the primary and secondary native hardware I2C buses provides a highly stable data tracking pipeline. Similarly, the alternating current consumption track managed by Node 2 effectively captures grid voltage variations and low-load appliance current signatures safely, which is a direct outcome of the physical 5-turn wire amplification loop moving micro-amperage properties clear of the chip's native hardware noise floor.

A primary focus of this discussion centers on how these distinct results interact to fulfill the core objectives of this research. By layering the real-time solar photovoltaic generation curve against individual appliance consumption parameters on a unified visual interface, the system directly addresses the residential behavior-action gap. Prosumers are no longer dependent on delayed monthly utility statements to understand their consumption footprints. Instead, they receive immediate graphical feedback detailing exactly how much energy a specific home appliance draws in relation to the active generation output of the solar array. This real-time visibility enables active, data-driven load-shifting habits, letting homeowners strategically schedule high-power tasks during peak solar harvest windows to increase direct self-consumption and maximize energy independence.

Furthermore, the data isolation achieved through the dual-node microcontroller layout addresses a critical structural issue identified in traditional home tracking architectures. By managing low-voltage direct current generation parameters on Node 1 while isolating single-phase alternating current appliance consumption lines on Node 2, the system eliminates the risk of high-frequency inverter switching harmonics or electromagnetic interference corrupting sensitive sensor bus lines. Offloading the temporal tracking burden from the edge microcontrollers to a server-side ingestion model similarly optimizes local runtime efficiency. Because clock indexing occurs entirely at the database write endpoint inside InfluxDB, the edge nodes operate as stateless, lightweight telemetry transmitters, protecting local memory arrays from the stability failures often induced by continuous network time protocol synchronization loops.

Despite these positive operational outcomes, the evaluation of the prototype reveals clear structural limitations that must be addressed. In the direct current generation path, the use of a standard 20A PWM charge controller introduces a significant efficiency bottleneck. A PWM controller acts as a direct electrical switch that binds the solar array directly to the battery storage reservoir. Because it lacks internal voltage-bucking conversion circuitry, it forces the operating voltage of the solar panel down to match the chemistry-driven potential of the 12V LiFePO4 battery bank. This voltage clamping prevents the solar panel from ever reaching its optimal maximum power point, capping total renewable generation efficiency. Additionally, the alternating current consumption node relies on a single plug-point interface topology, restricting sub-metering capacity to exactly one appliance terminal at a time rather than auditing multiple household branch circuits simultaneously.

CONCLUSION

The development of the dual-node residential solar-powered monitoring system successfully demonstrates an affordable, high-fidelity alternative to expensive proprietary energy management platforms. By separating the direct current renewable generation track from the single-phase alternating current appliance consumption interface across independent edge processing nodes, the architecture eliminates processing collisions and protects sensitive serial communication lines from high-frequency inverter noise. The implementation of a physical 5-turn wire amplification loop successfully overcomes the native hardware resolution constraints of non-invasive current clamps, allowing the system to accurately resolve low-power household standby footprints down to single-digit wattages.

The platform successfully shifts the resource-heavy burden of chronological clock tracking and temporal synchronization away from edge microcontrollers to a server-side ingestion model managed within an index-optimized time-series database. This middleware approach maintains precise millisecond logging timelines while protecting local edge hardware memory stacks from stability failures. Furthermore, the integration of throttled event-driven state machines provides low-latency proactive battery protections without flooding the user interface with redundant alert strings.

While the current prototype highlights clear engineering limitations regarding the clamping efficiency deficits of standard pulse width modulation controllers and the monitoring scope of a single-plug interface, it establishes a reliable baseline for open-source home energy management. Future iterations will focus on upgrading the renewable pathway to a maximum power point tracking stage to unlock full generation capacity, expanding the consumption node to handle multi-channel branch circuit sub-metering, and implementing true phase-angle processing to calculate reactive power footprints across inductive household motor loads.

ACKNOWLEDGEMENT

The authors would like to express their thanks to Faculty of Electronics and Computer Technology and Engineering (FTKEK) at Universiti Teknikal Malaysia Melaka (UTeM) for their assistance in acquiring the essential information and resources for the successful completion of the research. The authors would also like to extend their gratitude to their collaborators at Politeknik Port Dickson for the financial and scientific support they provided.

REFERENCES

1. T. Khafiso, C. Aigbavboa, and S. A. Adekunle, "Barriers to the adoption of energy management systems in residential buildings," Facilities, vol. 42, no. 15/16, pp. 107-125, Dec. 2024, doi: 10.1108/F-12-2023-0113.
2. M. Poyyamozhi, B. Murugesan, N. Rajamanickam, M. Shorfuzzaman, and Y. Aboelmagd, "IoT-A promising solution to energy management in smart buildings: A systematic review, applications, barriers, and future scope," Buildings, vol. 14, no. 11, p. 3446, Oct. 2024, doi: 10.3390/buildings14113446.

ISSN No. 2454-6186 | DOI: 10.47772/IJRISS | Volume X Issue VII July 2026

3. S. Corgnati, E. Guercio, and S. D'Oca, "Energy@home: Energy monitoring in everyday life," in Universal Access in Human-Computer Interaction. Aging and Assistive Environments, vol. 8515, C. Stephanidis and M. Antona, eds., in Lecture Notes in Computer Science, vol. 8515, Cham: Springer International Publishing, 2014, pp. 483-492, doi: 10.1007/978-3-319-07446-7_47.
4. N. A. Baidoo et al., "Households' energy conservation and efficiency awareness practices in the Cape Coast Metropolis of Ghana," Discov. Sustain., vol. 5, no. 1, p. 2, Jan. 2024, doi: 10.1007/s43621-023-00154-6.
5. J. Zywiolek, J. Rosak-Szyrocka, and M. Mrowiec, "Knowledge management in households about energy saving as part of the awareness of sustainable development," Energies, vol. 14, no. 24, p. 8207, Dec. 2021, doi: 10.3390/en14248207.
6. B. Vaidya, K. R. Panthee, and J. Amgain, "Awareness of household energy consumption and its impact on the environment: A case of Kathmandu Valley, Nepal," J. Econ. Concerns, vol. 13, no. 1, pp. 24-36, Dec. 2022, doi: 10.3126/tjec.v13i1.57059.
7. M. Dell'Isola, G. Ficco, L. Canale, B. Palella, and G. Puglisi, "An IoT integrated tool to enhance user awareness on energy consumption in residential buildings," Atmosphere, vol. 10, no. 12, p. 743, Nov. 2019, doi: 10.3390/atmos10120743.